HHS Public Access

Author manuscript

J Thromb Haemost. Author manuscript; available in PMC 2018 March 01.

Published in final edited form as:

J Thromb Haemost. 2017 March ; 15(3): 526–537. doi:10.1111/jth.13600.

Hierarchical organization of the hemostatic response to penetrating injuries in the mouse macrovasculature

John D. Welsh[1,2], **Izmarie Poventud-Fuentes**[1], **Sara Sampietro**[1], **Scott L. Diamond**[2], **Timothy J. Stalker**[1], and **Lawrence F. Brass**[1]

[1]Departments of Medicine and Pharmacology, University of Pennsylvania, Philadelphia, PA

[2]Department of Chemical and Biomolecular Engineering, University of Pennsylvania, Philadelphia, PA

Summary

Background—Intravital studies performed in the mouse microcirculation show that hemostatic thrombi formed after penetrating injuries develop a characteristic architecture in which a core of fully-activated, densely-packed platelets is overlaid with a shell of less activated platelets.

Objective—Large differences in hemodynamics and vessel wall biology distinguish arteries from arterioles. Here we asked whether these differences affect the hemostatic response and alter the impact of anticoagulants and antiplatelet agents.

Methods—Approaches previously developed for intravital imaging in the mouse microcirculation were adapted to the femoral artery, enabling real time fluorescence imaging despite the markedly thicker vessel wall.

Results—Arterial thrombi initiated by penetrating injuries developed the core-and-shell architecture previously observed in the microcirculation. However, although platelet accumulation was greater in arterial thrombi, the kinetics of platelet activation were slower. Inhibiting platelet ADP $P2Y_{12}$ receptors destabilized the shell and reduced thrombus size without affecting the core. Inhibiting thrombin with hirudin suppressed fibrin accumulation, but had little impact on thrombus size. Removing the platelet collagen receptor, glycoprotein VI, had no effect.

Conclusions—These results 1) demonstrate the feasibility of performing high speed fluorescence imaging in larger vessels and 2) highlight differences as well as similarities in the hemostatic response in the macro- and microcirculation. Similarities include the overall core-and-shell architecture. Differences include the slower kinetics of platelet activation and a smaller contribution from thrombin, which may be due in part to the greater thickness of the arterial wall and the correspondingly greater separation of tissue factor from the vessel lumen.

Corresponding Author: Lawrence F. Brass, MD/PhD, University of Pennsylvania, Perelman School of Medicine, 815 BRB II/III, 421 Curie Blvd, Philadelphia, PA 19104, brass@mail.med.upenn.edu, Ph: 215-573-3540.

Authorship

J. D. Welsh. designed and conducted the experiments, analyzed data, and wrote the manuscript. I. Poventud-Fuentes and S. Sampietro conducted experiments and analyzed data. T. J. Stalker, S. L. Diamond and L. F. Brass analyzed data and wrote the manuscript.

Keywords

Platelet Activation; Platelet Aggregation Inhibitors; Thrombin; Fibrin; Thromboplastin

Introduction

Following penetrating vascular injuries, hemostatic thrombi form to limit blood loss. In recent studies, we and others have examined platelet activation and fibrin accumulation following penetrating injuries in the mouse microvasculature, focusing on the hemostatic response rather than pathological occlusive thrombosis initiated either by stasis or chemical irritants such as $FeCl_3$ [1-5]. Our studies were performed in arterioles and venules using high-resolution confocal fluorescence microscopy in combination with biosensors that measure thrombin activity, platelet packing density, intrathrombus transport and the rate of protein loss at the site of injury. The biosensors helped to define critical properties of the hemostatic mass along with the activation state of platelets within the mass [2, 6-10].

The results of those studies showed that hemostatic thrombi in the microcirculation consist of a relatively small amount of fibrin at the injury site covered by a larger accumulation of platelets. Rather than a mass of fully activated platelets evenly interspersed with fibrin, hemostatic thrombi formed in this setting developed a characteristic architecture in which a core of densely-packed, highly-activated platelets is overlaid with a shell of less activated, loosely-packed platelets, with the difference between the two regions functionally defined by the presence or absence of the α-granule membrane protein, P-selectin, on the platelet surface [2, 11]. The results also showed that the structure of the hemostatic mass is shaped by gradients of soluble platelet agonists that are determined in part by the slowness of solute transport in the narrowing gaps between platelets, especially in the tightly-packed platelet core [7-9]. Collectively, the results suggested that the hemostatic response in the microvasculature is shaped not only by the attributes of individual platelets, but also by properties of the system as a whole that emerge as platelets accumulate and, by the simple act of piling up, alter their local environment. We have suggested that these emergent properties help to limit overall thrombus growth and prevent unnecessary vascular occlusion. Much of this work was performed in mouse models, but key features were confirmed with human blood studied in microfluidics devices [11, 12].

Here we consider whether the lessons learned from studies in the microvasculature carry over to larger vessels, which is where much human disease occurs, especially in the coronary, cerebral and peripheral arterial circulations. For technical reasons related in part to vessel wall thickness, high resolution fluorescence imaging of the hemostatic response in mouse models has primarily been limited to the microvasculature, usually in the cremaster muscle or the intestinal mesentery. The macrocirculation differs from the microcirculation significantly in vessel wall structure [13-19] and local hemodynamics [20-22]. These differences have been shown to affect the underlying molecular mechanisms driving platelet activation and thrombus formation in different vascular beds [23-26]. Here we asked whether these differences also re-shape the hemostatic response, affecting thrombus structure, changing emergent properties and altering the impact of anticoagulant drugs and antiplatelet agents.

To answer these questions, high-resolution, real time confocal fluorescence imaging techniques were adapted for use in the femoral artery, and methods were developed to obtain reproducible penetrating injuries.

The results show that in the femoral artery hemostatic thrombi develop a complex structure with regions of greater and lesser platelet activation, much as they do in arterioles. However, total platelet accumulation is considerably greater in the femoral artery and the kinetics of P-selectin appearance on the platelet surface are slower. Parallel studies in femoral veins suggest that the differences in kinetics apply to veins as well. As in arterioles, inhibiting platelet responses to ADP by blocking $P2Y_{12}$ receptors destabilized the shell region and reduced overall thrombus size without affecting the core region. In contrast, inhibiting thrombin had proportionately less of an effect on total platelet deposition than in arterioles, suggesting that other factors are important as well, including the greater separation of tissue factor from the vessel lumen [27].

Collectively these results 1) demonstrate the feasibility of performing high speed fluorescence imaging in arteries and veins with walls that are thicker those in arterioles and venules, and 2) show that there are differences as well as similarities in the hemostatic response to penetrating injuries in the macro- and microcirculation. The similarities include the overall core-and-shell architecture observed in both settings. The differences include the slower kinetics of platelet activation and the reduced impact of thrombin inhibitors.

Methods

Materials

C57Bl/6J mice 8-12 weeks old were used for all experiments (Jackson Laboratories, Bar Harbor, ME, USA). Thrombus formation was visualized using anti-CD62P (IgG, clone RB40.34) and anti-CD41 ($F(ab)_2$ fragment, clone MWReg30) (BD Biosciences, San Diego, CA, USA). Fluorescent fibrinogen conjugated to AlexaFluor 488 provided information about fibrin(ogen) deposition (Life Technologies, Grand Island, NY, USA). Thrombus formation was modified by the infusion of cangrelor (a gift from The Medicines Company) or hirudin (a gift from Dr. Sriram Krishnaswamay, Children's Hospital of Philadelphia).

Femoral artery and vein visualization

All procedures were reviewed and approved by the University of Pennsylvania Perelman School of Medicine IACUC. Mice were anesthetized with an intraperitoneal injection of either sodium pentobarbital (90 mg/kg) or ketamine/xylazine/acepromazine (100/10/3 mg/kg, respectively). The mouse jugular vein was then cannulated for the infusion of anti-CD41 (3 μg), anti-CD62P (5 μg), and fluorescent fibrinogen (50 μg) to visualize thrombus formation. When indicated in the text, cangrelor (75 μg) and hirudin (30 μg/kg or 0.75 μg in a 25 g mouse) were infused immediately before each injury.

To observe hemostatic thrombus formation, we exteriorized the femoral artery and vein, removed overlaying connective tissue, and constantly perfused bicarbonate buffer (37 °C, bubbled with 95%/5% N_2CO_2) to facilitate imaging with a 40X water immersion objective (Olympus, St. Louis, MO, USA). Vessel injury was induced with a pulsed nitrogen dye laser

(SRS NL100, 440nm) focused on the vessel wall. The laser was pulsed until red cell loss had occurred. Blood loss lasted for only a few seconds after injury, ending before image capture could be initiated.

Hemostatic thrombi were imaged with a BX61WI microscope (Olympus, St. Louis, MO, USA) and a CSU-X1 spinning disk confocal scanner (Yokogawa) capturing a top down view of the forming thrombus in which the vessel wall and the thrombus core were closer to the microscope objective lens than the thrombus shell (Figure 1A). Fluorescence imaging was performed using a set of diode pumped solid state lasers with acousto-optic tunable filter control as an excitation source (LaserStack; Intelligent Imaging Innovations). Images were captured with an Evolve digital camera (Photometrics).

Image analysis

The maximum background fluorescence signal for each channel was measured within the thrombus-free portion of the lumen within the same field of view as the thrombus. The image was then converted to a binary mask of all pixels above that maximum and either the area (μm^2) or sum fluorescence intensity (FI 10^6 RFU) from that mask were measured for each mask after background subtraction.

Real time tracking of mask area and fluorescence intensity allowed for us to quantify 3 distinct metrics: initial growth rate (over 60 s for thrombus area, and 20 s for fibrinogen deposition as they were typical ranges of the linear phase of growth), peak thrombus/P-selectin area and fibrinogen fluorescence intensity, and final thrombus/P-selectin area and fibrinogen fluorescence intensity. We then performed statistical analysis on these metrics using the Mann-Whitney U test.

Immunohistochemistry

Mouse femoral arteries were isolated without perfusion, briefly washed with 1x PBS and fixed with 4% formalin for 4 hours. Tissue was dehydrated, processed for paraffin embedding, and sectioned (5 μm). After paraffin removal and rehydration, antigen retrieval was done with citrate buffer (10 mM, pH 6) for 20 minutes, after which peroxidase activity was blocked with 3% H_2O_2 for 20 minutes. Sections were blocked with 2% normal rabbit serum (Vector Laboratories: S-5000) for 15 minutes and with Avidin/Biotin Blocking Kit (Vector Laboratories: SP-2001) as suggested by manufacturer. Primary antibody incubation was done overnight at 4°C at a dilution of 1:200 for tissue factor (R&D: AF3178) and 1:150 for PECAM-1 (Santa Cruz: sc-1506). Sections were incubated with biotinylated rabbit anti-goat IgG antibody (Vector Laboratories: BA-5000) at a 1:1000 dilution for 45 minutes and with Vector Elite ABC kit (Vector Laboratories: PK-6200) as specified by manufacturer. Staining was developed with DAB substrate (Dako: K3467), counterstaining with hematoxylin, and mounting with Cytoseal-60 (Richard-Allan Scientific: 8310-4). Pictures were taken at 40x magnification using a Nikon Eclipse 80i microscope with a QImaging Micropublisher 5.0 RTV camera. Using Image J, binary masks of the tissue factor positive area were made. The vessel lumen was outlined and the percentage of positive area within concentric circles of known distance from the lumen was calculated. For each vessel, 10

measurements gave the distribution of tissue factor up to 100 μm from the lumen. For each group (femoral artery and cremaster arteriole), 5 different vessels were quantified.

Depleting GPVI from platelets

Mice were injected in the retro-orbital plexus with 100 μg Jaq-1 GPVI depletion antibody (Emfret Analytics. Eibelstadt, Germany) for 4-5 days. Depletion of GPVI was confirmed by measurement of JON/A (PE, Emfret Analytics, Eibelstadt, Germany) binding to platelets stimulated with either the GP VI agonist, convulxin (0.6 μg/mL), or the PAR4 agonist peptide, AYPGKF (200 μM), from either Jaq-1- or vehicle-treated mice. JON/A binding was measured using a BD FACSCanto cytofluorimeter. Data were acquired with BD FACSDiva software and analyzed with FlowJo v10.

Results

Thrombus architecture and kinetics in the femoral artery

After surgical exposure of the femoral artery, a through-and-through penetrating injury was made with a nitrogen dye laser. Laser pulses were continued until red cell escape was observed (Figure 1A and B). The resultant hole was approximately 15-20 μm across. This is smaller than was produced in a recent study on mouse saphenous veins (50-100 μm diameter) [26] in which the experimental goals were different and blood loss was prolonged. Here our goal was to observe the hemostatic response under conditions comparable at a functional level to those that we and others have employed in the microcirculation [2]. In both injury models the loss of red cells ended within seconds of turning off the laser, but a more substantial injury was required to induce bleeding from femoral arteries due to their thicker vessel wall [6]. Platelet deposition (CD41) and P-selectin exposure were recorded in real time. Fluorescent fibrinogen was used to track fibrin accumulation because we found that fibrin-specific antibodies did not have full access to fibrin deposited within the arterial wall. We believe the fibrin(ogen)-related fluorescence that we observed is largely due to fibrin rather than fibrinogen since, as will be shown, adding a thrombin inhibitor largely eliminated the signal.

The results in Figure 1C show that there was rapid platelet accumulation around the injury site with a large mass present 60 s after the injury. P-selectin translocation to the platelet surface following α-granule secretion took longer, becoming detectable after about 60 s, then gradually increasing over the next several minutes to form a substantial core region that was visible after 5 minutes and well defined after 20 minutes. During that same time period the platelet mass became more aligned with the flow. Concurrently, fibrin was deposited at the injury site and spread perpendicularly to flow within the vessel wall (Figure 1D and E). Notably, the thrombus core, defined as P-selectin(+) platelets [2], formed largely within the vessel wall, while the P-selectin(−) shell formed within the vessel lumen, starting on top of the core and extending downstream (Figure 1C-E). This hierarchical structure is especially visible when a 3D reconstruction of a series of confocal z-plane images is rotated digitally to give a view from the side (Figure 1E).

Comparative kinetics in the micro- and macrocirculations

To directly compare the kinetics of thrombus growth and core formation in the femoral artery with the response in cremaster muscle arterioles, we performed injuries in both. An example in the cremaster muscle is shown in Supplemental Figure S1[1]. The laser injury resulted in brief period of red cell loss (<5 s) in both vasculatures, suggesting a comparable level of injury relative to vessel size. In response to the femoral artery injury, platelets accumulated rapidly, peaking between 20-45 s after injury (Figure 2A). P-selectin exposure increased continuously over 300 seconds, while fibrin(ogen) accumulation leveled off within 60 seconds (Figure 2A-D). Although total platelet deposition was considerably greater in the femoral artery (compare Figure 2A with Figure 2C), the time to peak thrombus size was approximately the same (Figure 2E). In contrast, while core size was also greater in the artery than the arterioles, the rate of core formation was slower (Figure 2F and G) and fibrin(ogen) accumulation was smaller, as was the proportion of platelets became P-selectin(+) during the observation period (compare Figure 2A&B with Figure 2C&D).

Taken together, these results demonstrate that penetrating injuries in both the macro- and microcirculation leads to stable hemostatic thrombus formation marked by the appearance of a core-and-shell architecture. The rate of platelet accumulation in the arteries is greater than in the arterioles, but the kinetics of P-selectin exposure are slower. Parallel observations in the femoral vein produced similar results (Supplemental Figure S2).

The role of thrombin

To investigate the role of thrombin in arterial injuries, we infused the direct-acting thrombin inhibitor, hirudin. Despite essentially abolishing fibrin(ogen) accumulation, hirudin had no effect on overall platelet accumulation (Figure 3A-C). However, hirudin did significantly decrease P-selectin exposure, leading to an approximately 60% reduction in core size 5 minutes after injury (Figure 3D).

These results suggest that while full platelet activation in the femoral artery (defined by P-selectin expression) is clearly thrombin-dependent, platelet accumulation in this particular injury model is less thrombin-dependent than in cremaster muscle arterioles. To try to understand this difference, we examined the distribution of tissue factor around the femoral artery and cremaster muscle arterioles [13, 28, 29]. The results showed that tissue factor was primarily localized to the adventitia in both the macro- and microcirculation (Figure 4A&B and reference [27]). However, the distance from lumen to tissue factor was substantially greater in the femoral artery than in cremaster muscle arterioles (Figure 4C). This difference may delay thrombin generation and/or diffusion, leading to the observed delay in core formation and the localization of fibrin and P-selectin(+) platelets within the vessel wall (Figure 1C&D).

[1]Note that it is possible to obtain bright field imaging in the exposed cremaster muscle, which can be exteriorized and placed on the microscope stage, but not in the femoral artery.

The role of ADP

Activation of platelet $P2Y_{12}$ receptors by ADP is important for stable $\alpha_{IIb}\beta_3$ integrin activation and stable thrombus formation in cremaster muscle arterioles and the saphenous vein [2, 26, 30]. In the microcirculation, infusion of the direct acting $P2Y_{12}$ antagonist, cangrelor, strips away most of the platelets in the shell, but does not impact the size or activation level of the core region [2]. Here we observed that cangrelor has a very similar effect in the femoral artery, decreasing thrombus size and increasing embolization (Figure 5A-C; Supplemental video 1 and 2). However, cangrelor treatment only destabilized the downstream portion of the thrombus (seen in blue in Figure 5D). Hemostatic thrombi formed in the presence of cangrelor still formed a stable and hemostatic core region with no significant difference from vehicle treated thrombi (Figure 5E). These results show that the role of ADP in shaping hemostatic thrombus architecture is conserved across vascular beds.

Platelet GPVI signaling

Glycoprotein (GP) VI is the primary signaling receptor for collagen on mouse and human platelets. Others have observed that the importance of GPVI signaling during thrombus formation is dependent upon the mechanism and extent of injury. For injuries in which there is extensive endothelial cell denudation and collagen exposure, GPVI signaling is critical [31-34]. However, for penetrating injuries the increasing severity of the injury has been shown to increase the role of thrombin and lessen the contribution of GPVI [5, 31, 35, 36]. In the studies shown in Figure 6, mice were injected with the GPVI antibody, Jaq-1, which depletes GPVI from the platelet surface [37]. Loss of GPVI was documented by flow cytometry (Supplemental Figure S3), but had no apparent effect on either platelet accumulation or platelet activation. This suggests that GPVI-dependent collagen signaling plays a relatively small role in this injury model.

Discussion

Although the term “thrombus” is sometimes applied to both, hemostasis and thrombosis are very different processes. Efforts to develop mouse models that mimic either event in humans have produced an array of methods. Some of these focus on hemostasis, while others produce occlusive thrombi intended to mimic pathologic thrombosis [23-25, 38]. Here we have focused on hemostasis, asking whether the lessons learned from observing and modeling the hemostatic response in the microcirculation can be applied to the arterial macrocirculation, where the lumen is larger and flow rates are faster.

In the mouse microcirculation, hemostatic thrombi formed following penetrating injuries produced with a laser or a glass probe have been shown to be comprised of a core of densely-packed, fully-activated platelets with an overlying shell of less-activated platelets [2, 4, 28, 39]. Fibrin accumulation in this setting is limited to the thrombus core, as is platelet-associated thrombin activity [10]. Our previously-published data suggest that this is in part because the rapid accumulation of densely packed platelets in the thrombus core produces conditions in which the intrathrombus transport of soluble molecules such as thrombin is slowed to the point where it becomes diffusion-limited rather than convection-driven [8, 9]. Agonist concentration gradients form, radiating outward from the site of injury,

but falling off at rates that are relatively agonist-specific. Stable platelet accumulation in this model is primarily dependent on the thrombin produced following tissue factor exposure [2, 28, 29, 40, 41]. Secondary growth is driven by ADP and TxA_2 released by activated platelets and damaged cells [2, 42]. This leads to a stable hemostatic thrombus marked by a core-and-shell architecture, heterogeneity in the extent of platelet activation and differences in packing density [2].

Methods to perform comparable real time, high resolution intravital fluorescence imaging in the mouse macrovasculature have previously been limited by the greater wall thickness in arteries and veins compared to arterioles and venules, making it harder to see what is happening. To determine how agonist generation and activity shape the hemostatic response in the macrovasculature, here we have developed methods adapted for use in the mouse femoral artery and vein. The results were compared with injuries made in cremaster muscle arterioles. In both settings, the extent of injury was adjusted so that the duration of red cell escape was brief, stopping well before platelet accumulation had peaked. Given its greater wall thickness, this meant that the extent of injury was greater in the femoral artery studies, accounting in part for the greater size of the thrombus.

The results highlight similarities as well as differences between the hemostatic response in the macro- and microcirculation. Most notably, the core-and-shell architecture observed in arterioles and venules also proved to be present in the femoral artery and vein. The relative rates of thrombus growth were similar, with the rapid initial phase of platelet accumulation reaching its limit approximately 60 seconds after injury despite the differences in local hydrodynamics. Inhibiting ADP $P2Y_{12}$ receptors reduced shell stability and decreased thrombus growth, but did not affect formation of the core region. This effect was similar to that observed in cremaster arterioles and venules [6]. It suggests why orally-active $P2Y_{12}$ antagonists have proved to be so successful in preventing occlusive thrombus formation in the setting of atherosclerotic vascular disease, while having relatively limited effects on hemostasis and bleeding risk.

Events in the femoral artery did not, however, entirely parallel those in arterioles. In addition to larger thrombus size, we observed differences in the kinetics of platelet accumulation, the kinetics of platelet activation and the distribution of degranulated (i.e. P-selectin positive) platelets. Although the time to peak thrombus size was similar in the macro- and microcirculation, femoral artery thrombi were much larger, which means that the number of platelets joining the thrombus per unit time was greater. There was also a difference in thrombus morphology. In the microcirculation where flow rates are slower and the vessel wall is thinner, hemostatic thrombi tend to project into the vessel lumen (Figure 7). Hemostatic thrombi formed in the femoral artery tended to be flatter and the P-selectin(+) platelets were largely confined to the injury site within the vessel wall, which is also where most of the fibrin was found. This suggests that thrombin production occurs primarily within the wall, the region of the thrombus that is closest to the adventitia where tissue factor is expressed.

Core formation in the cremaster artery injury model is primarily driven by thrombin [2, 43]. The data reported here show that in the femoral artery inhibition of thrombin with hirudin

reduced the size of the thrombus core, but had little effect on total platelet accumulation. This suggests that thrombin is driving platelet degranulation, but it is not the primary driver for platelet accumulation. ADP makes up part of the difference. Platelet-derived TxA_2 presumably contributes as well, although that has not been addressed in this setting. GPVI - dependent collagen signaling, on the other hand, appears to be dispensable in this model.

Notably, in their studies of bleeding caused by repeated injuries in saphenous veins, Getz *et al.* showed that mice with reduced tissue factor expression do not have a hemostatic defect in response to a single laser induced vessel rupture [26], which also suggests a limited role for thrombin. In mesenteric arteries thrombin activity has been shown to be dependent upon injury severity [5, 31, 36], with the response to milder injuries being driven by thrombin plus collagen and severe injuries being largely thrombin dependent [5]. As the vessel wall grows thicker, not only is tissue factor farther away from the lumen, but any thrombin that is formed has a greater distance to diffuse in the tortuous path produced by the narrowing gaps between adjoining platelets (Figure 7). This environment promotes thrombin accumulation, but also limits its spread [7-9]. This may account for our observation that a smaller proportion of the platelets in the thrombus became P-selectin(+) and hirudin had little impact on total platelet accumulation in the femoral artery compared to cremaster muscle arterioles.

In summary, here we have described a novel method for observing the hemostatic response in the mouse femoral artery that overcomes some of the previous limitations to performing fluorescence intravital microscopy in larger vessels with their thicker walls. These injuries are comparable to the those that we and others have produced in the cremaster microcirculation, and thus provide a method to measure the impact of changing vessel biology and hemodynamics on the hemostatic process. The results show that the core-and-shell architecture of hemostatic thrombi is largely, but not entirely, conserved throughout both the macro- and microcirculation, suggesting that this architecture plays an important role in establishing hemostasis. In both cases the structure of the hemostatic mass appears to be very different from the structure of pathological thrombi. We propose that this technique will prove informative in understanding events in clinically-relevant vascular diseases, including atherothrombosis.

Supplementary Material

Refer to Web version on PubMed Central for supplementary material.

Acknowledgements

This work was supported by the National Heart, Lung and Blood Institute (P01 HL40387 and P01 HL120846 to T. J. Stalker and L. F. Brass, and R01 HL103419 to S. L. Diamond and L. F. Brass.). J. D. Welsh was supported by American Heart Association predoctoral fellowship 14PRE19560005 and NIH T32 HL07439. I. Poventud-Fuentes was supported by NIH T32 GM008076. The spinning disk confocal microscopy system employed was partially funded by NIH-NCRR S10 RR26716-1.

References

1. Furie B, Furie BC. Thrombus formation in vivo. J Clin Invest. 2005; 115:3355–62. [PubMed: 16322780]

2. Stalker TJ, Traxler EA, Wu J, Wannemacher KM, Cermignano SL, Voronov R, Diamond SL, Brasset LF. Hierarchical organization in the hemostatic response and its relationship to the platelet-signaling network. Blood. 2013; 121:1875–85. [PubMed: 23303817]

3. Ivanciu L, Krishnaswamy S, Camire RM. New insights into the spatiotemporal localization of prothrombinase in vivo. Blood. 2014; 124:1705–14. [PubMed: 24869936]

4. Kamocka MM, Mu J, Liu X, Chen N, Zollman A, Sturonas-Brown B, Dunn K, Xu Z, Chen DZ, Alber MS, Rosen ED. Two-photon intravital imaging of thrombus development. Journal of biomedical optics. 2010; 15:0160201–7.

5. Hechler B, Nonne C, Eckly A, Magnenat S, Rinckel JY, Denis CV, Freund M, Cazenave JP, Lanza F, Gachet C. Arterial thrombosis: relevance of a model with two levels of severity assessed by histologic, ultrastructural and functional characterization. J Thromb Haemost. 2010; 8:173–84. [PubMed: 19874458]

6. Welsh JD, Muthard RW, Stalker TJ, Taliaferro JP, Diamond SL, Brass LF. A systems approach to hemostasis: 4. How hemostatic thrombi limit the loss of plasma-borne molecules from the microvasculature. Blood. 2016; 127:1598–605. [PubMed: 26738537]

7. Welsh JD, Stalker TJ, Voronov R, Muthard RW, Tomaiuolo M, Diamond SL, Brass LF. A systems approach to hemostasis: 1. The interdependence of thrombus architecture and agonist movements in the gaps between platelets. Blood. 2014; 124:1808–15. [PubMed: 24951424]

8. Tomaiuolo M, Stalker TJ, Welsh JD, Diamond SL, Sinno T, Brass LF. A systems approach to hemostasis: 2. Computational analysis of molecular transport in the thrombus microenvironment. Blood. 2014; 124:1816–23. [PubMed: 24951425]

9. Stalker TJ, Welsh JD, Tomaiuolo M, Wu J, Colace TV, Diamond SL, Brass LF. A systems approach to hemostasis: 3. Thrombus consolidation regulates intrathrombus solute transport and local thrombin activity. Blood. 2014; 124:1824–31. [PubMed: 24951426]

10. Welsh JD, Colace TV, Muthard RW, Stalker TJ, Brass LF, Diamond SL. Platelet-targeting sensor reveals thrombin gradients within blood clots forming in microfluidic assays and in mouse. J Thromb Haemost. 2012; 10:2344–53. [PubMed: 22978514]

11. Muthard RW, Diamond SL. Side view thrombosis microfluidic device with controllable wall shear rate and transthrombus pressure gradient. Lab Chip. 2013; 13:1883–91. [PubMed: 23549358]

12. Muthard RW, Diamond SL. Blood clots are rapidly assembled hemodynamic sensors: flow arrest triggers intraluminal thrombus contraction. Arterioscler Thromb Vasc Biol. 2012; 32:2938–45. [PubMed: 23087356]

13. Kretz CA, Vaezzadeh N, Gross PL. Tissue factor and thrombosis models. Arterioscler Thromb Vasc Biol. 2010; 30:900–8. [PubMed: 20393156]

14. Khan AI, Kerfoot SM, Heit B, Liu L, Andonegui G, Ruffell B, Johnson P, Kubes P. Role of CD44 and hyaluronan in neutrophil recruitment. J Immunol. 2004; 173:7594–601. [PubMed: 15585887]

15. Figueroa XF, Chen CC, Campbell KP, Damon DN, Day KH, Ramos S, Dulin BR. Are voltage-dependent ion channels involved in the endothelial cell control of vasomotor tone? Am J Physiol Heart Circ Physiol. 2007; 293:H1371–83. [PubMed: 17513486]

16. Mui KL, Bae YH, Gao L, Liu SL, Xu T, Radice GL, Chen CS, Assoian RK. N-Cadherin Induction by ECM Stiffness and FAK Overrides the Spreading Requirement for Proliferation of Vascular Smooth Muscle Cells. Cell Rep. 2015; 10:1477–86.

17. Isakson BE, Best AK, Duling BR. Incidence of protein on actin bridges between endothelium and smooth muscle in arterioles demonstrates heterogeneous connexin expression and phosphorylation. Am J Physiol Heart Circ Physiol. 2008; 294:H2898–904. [PubMed: 18408134]

18. Saito T, Hasegawa Y, Ishigaki Y, Yamada T, Gao J, Imai J, Uno K, Kaneko K, Ogihara T, Shimosawa T, Asano T, Fujita T, Oka Y, Katagiri H. Importance of endothelial NF-kappaB signalling in vascular remodelling and aortic aneurysm formation. Cardiovascular research. 2013; 97:106–14. [PubMed: 23015640]

19. Schafer SC, Pellegrin M, Wyss C, Aubert JF, Nussberger J, Hayoz D, Lehr HA, Mazzolai L. Intravital microscopy reveals endothelial dysfunction in resistance arterioles in Angiotensin II-induced hypertension. Hypertension research : official journal of the Japanese Society of Hypertension. 2012; 35:855–61. [PubMed: 22573204]

20. Dietzel S, Pircher J, Nekolla AK, Gull M, Brändli AW, Pohl U, Rehberg M. Label-free determination of hemodynamic parameters in the microcirculaton with third harmonic generation microscopy. PloS one. 2014; 9:e99615. [PubMed: 24933027]
21. Wang CH, Chen KT, Mei HF, Lee JF, Cherng WJ, Lin SJ. Assessment of mouse hind limb endothelial function by measuring femoral artery blood flow responses. J Vasc Surg. 2011; 53:1350–8. [PubMed: 21276693]
22. Hong G, Lee JC, Robinson JT, Raaz U, Xie L, Huang NF, Cooke JP, Dai H. Multifunctional in vivo vascular imaging using near-infrared II fluorescence. Nat Med. 2012; 18:1841–6. [PubMed: 23160236]
23. Denis CV, Wagner DD. Platelet adhesion receptors and their ligands in mouse models of thrombosis. Arterioscler Thromb Vasc Biol. 2007; 27:728–39. [PubMed: 17272754]
24. Rumbaut RE, Slaff DW, Burns AR. Microvascular thrombosis models in venules and arterioles in vivo. Microcirculation. 2005; 12:259–74. [PubMed: 15814435]
25. Cooley BC. Murine arterial thrombus induction mechanism influences subsequent thrombodynamics. Thromb Res. 2015; 135:939–43. [PubMed: 25764909]
26. Getz TM, Piatt R, Petrich BG, Monroe D, Mackman N, Bergmeier W. Novel mouse hemostasis model for real-time determination of bleeding time and hemostatic plug composition. J Thromb Haemost. 2015; 13:417–25. [PubMed: 25442192]
27. Drake TA, Morrissey JH, Edgington TS. Selective cellular expression of tissue factor in human tissues. Implications for disorders of hemostasis and thrombosis. Am J Pathol. 1989; 134:1087–97. [PubMed: 2719077]
28. Falati S, Gross P, Merrill-Skoloff G, Furie BC, Furie B. Real-time in vivo imaging of platelets, tissue factor and fibrin during arterial thrombus formation in the mouse. Nat Med. 2002; 8:1175–81. [PubMed: 12244306]
29. Falati S, Liu Q, Gross P, Merrill-Skoloff G, Chou J, Vandendries E, Celi A, Croce K, Furie BC, Furie B. Accumulation of tissue factor into developing thrombi in vivo is dependent upon microparticle P-selectin glycoprotein ligand 1 and platelet P-selectin. J Exp Med. 2003; 197:1585–98. [PubMed: 12782720]
30. Stolla M, Stefanini L, Roden RC, Chavez M, Hirsch J, Greene T, Ouellette TD, Maloney SF, Diamond SL, Poncz M, Woulfe DS, Bergmeier W. The kinetics of {alpha}IIb{beta}3 activation determines the size and stability of thrombi in mice: implications for antiplatelet therapy. Blood. 2011; 117:1005–13. [PubMed: 20971951]
31. Dubois C, Panicot-Dubois L, Merrill-Skoloff G, Furie B, Furie BC. Glycoprotein VI-dependent and-independent pathways of thrombus formation in vivo. Blood. 2006; 107:3902–6. [PubMed: 16455953]
32. Massberg S, Gawaz M, Gruner S, Schulte V, Konrad I, Zohlnhöfer D, Heinzmann U, Nieswandt B. A crucial role of glycoprotein VI for platelet recruitment to the injured arterial wall in vivo. J Exp Med. 2003; 197:41–9. [PubMed: 12515812]
33. Massberg S, Konrad I, Bultmann A, Schulz C, Münch G, Peluso M, Lorenz M, Schneider S, Besta F, Müller I, Hu B, Langer H, Kremmer E, Rudelius M, Heinzmann U, Ungerer M, Gawaz M. Soluble glycoprotein VI dimer inhibits platelet adhesion and aggregation to the injured vessel wall in vivo. Faseb J. 2004; 18:397–9. [PubMed: 14656994]
34. Munnix IC, Strehl A, Kuijpers MJ, Auger JM, van der Meijden PE, van Zandvoort MA, oude Egbrink MG, Nieswandt B, Heemskerk JW. The glycoprotein VI-phospholipase Cgamma2 signaling pathway controls thrombus formation induced by collagen and tissue factor in vitro and in vivo. Arterioscler Thromb Vasc Biol. 2005; 25:2673–8. [PubMed: 16254207]
35. Mangin P, Yap CL, Nonne C, Sturgeon SA, Goncalves I, Yuan Y, Schoenwaelder SM, Wright CE, Lanza F, Jackson SP. Thrombin overcomes the thrombosis defect associated with platelet GPVI/FcRgamma deficiency. Blood. 2006; 107:4346–53. [PubMed: 16391010]
36. Kalia N, Auger JM, Atkinson B, Watson SP. Critical role of FcR gamma-chain, LAT, PLCgamma2 and thrombin in arteriolar thrombus formation upon mild, laser-induced endothelial injury in vivo. Microcirculation. 2008; 15:325–35. [PubMed: 18464161]

37. Nieswandt B, Schulte V, Bergmeier W, Mokhtari-Nejad R, Rackebrandt K, Cazenave JP, Ohlmann P, Gachet C, Zirngibl H. Long-term antithrombotic protection by in vivo depletion of platelet glycoprotein VI in mice. J Exp Med. 2001; 193:459–69. [PubMed: 11181698]

38. Denis CV, Dubois C, Brass LF, Heemskerk JW, Lenting PJ, Biorheology Subcommittee of the SSCotI. Towards standardization of in vivo thrombosis studies in mice. J Thromb Haemost. 2011; 9:1641–4. [PubMed: 21585649]

39. Falati S, Gross PL, Merrill-Skoloff G, Sim D, Flaumenhaft R, Celi A, Furie BC, Furie B. In vivo models of platelet function and thrombosis: study of real-time thrombus formation. Methods Mol Biol. 2004; 272:187–97. [PubMed: 15226545]

40. Milanov P, Ivanciu L, Abriss D, Quade-Lyssy P, Miesbach W, Alesci S, Tonn T, Grez M, Seifried E, Schüttrumpf J. Engineered factor IX variants bypass FVIII and correct hemophilia A phenotype in mice. Blood. 2012; 119:602–11. [PubMed: 22031860]

41. Ivanciu L, Toso R, Margaritis P, Pavani G, Kim H, Schlachterman A, Liu JH, Clerin V, Pittman DD, Rose-Miranda R, Shields KM, Erbe DV, Tobin JF, Arruda VR, Camire RM. A zymogen-like factor Xa variant corrects the coagulation defect in hemophilia. Nat Biotechnol. 2011; 29:1028–33. [PubMed: 22020385]

42. Yang F, Shen Y, Yu Y, Stalker TJ, Zhu L. Thromboxane A2 Signaling Regulates Heterogeneous Platelet Activation Following Laser-Induced Injury In Mouse Cremaster Arterioles. Blood. 2013; 122:1055.

43. Vandendries ER, Hamilton JR, Coughlin SR, Furie B, Furie BC. PAR4 is required for platelet thrombus propagation but not fibrin generation in a mouse model of thrombosis. Proc Natl Acad Sci U S A. 2007; 104:288–92. [PubMed: 17190826]

Essentials

1. Methods were developed to image the hemostatic response in mouse femoral arteries in real time.
2. Penetrating injuries produced thrombi consisting primarily of platelets.
3. Alike to arterioles, a core-shell architecture of platelet activation occurs in the femoral artery.
4. Differences from arterioles included slower platelet activation and reduced thrombin dependence.

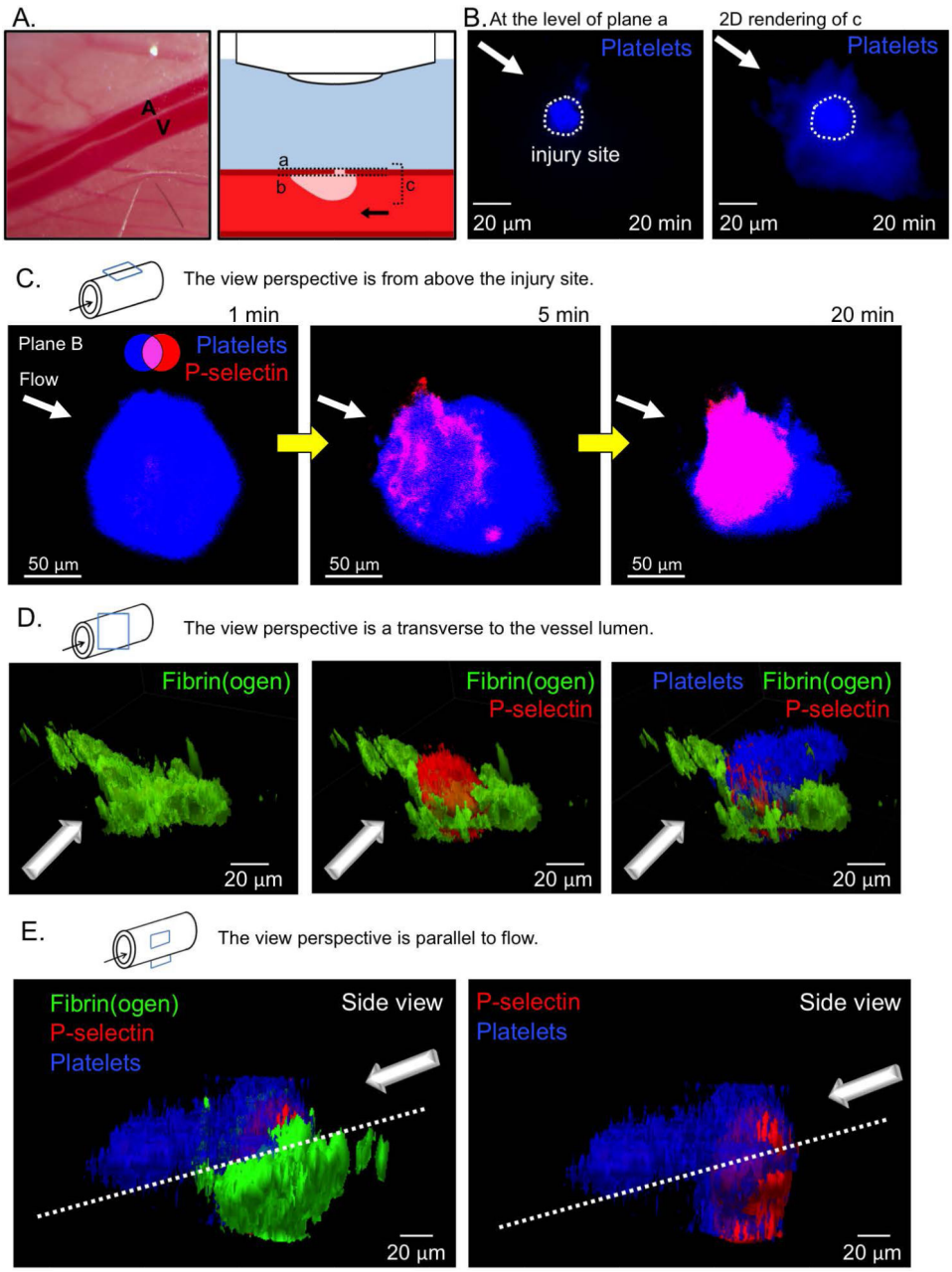

Figure 1. Laser injury of the mouse femoral artery

(A) A representative image of the mouse femoral artery (A) and vein (V), and schematic of microscope orientation to the vessel and injury site, and the various focal planes used for imaging (A-C). Note that the site of injury and, therefore, the thrombus core are closer to the microscope objective than the thrombus shell. (B) Representative images of the resulting thrombus (blue) 20 minutes post-injury. A confocal slice at the vessel wall (plane a, left) shows the injury site area, and the compressed 3D stack of the thrombus (plane c, right) shows the full size of the resulting thrombus. Plane b is at the inner surface of the vessel wall. (C) A time course of representative images showing platelet accumulation (blue) and P-selectin exposure (red) following laser injury. (D) A 3D rendering of a representative

thrombus showing fibrin(ogen) (green), P-selectin (red), and platelets (blue) 20 minutes post-injury from the front, and (E) from the side.

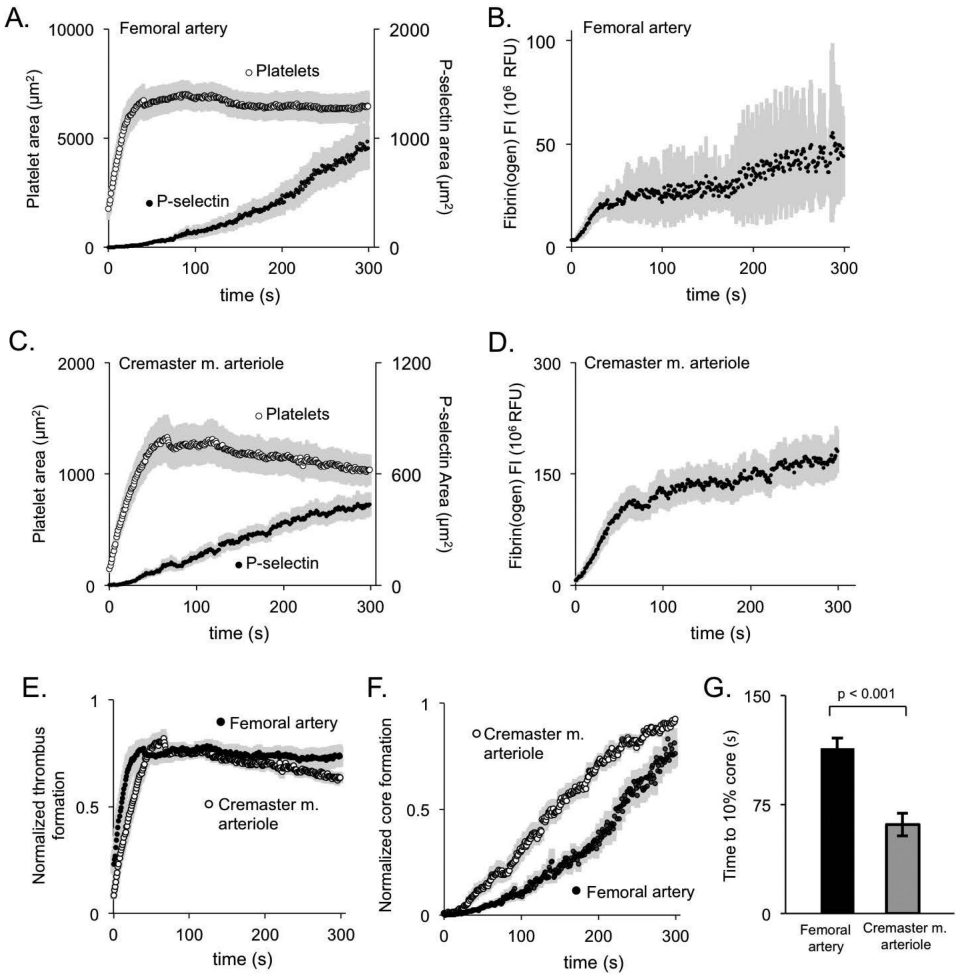

Figure 2. Comparison of thrombus kinetics in the macro- and microvasculature

(A,B) Quantitation of platelet area (open symbol), P-selectin(+) area (closed symbol), and fibrin(ogen) deposition following laser injury of the femoral artery (+/− SEM, n= 19). (C,D) The same endpoints in cremaster muscle arterioles (+/− SEM, n = 17). (E) Normalized thrombus area and (F) core area over time for femoral artery thrombi and cremaster muscle arterioles. Each individual thrombus was normalized so that its maximum thrombus area or core area was 1 and averaged (+/− SEM, n = 19 femoral and 17 cremaster). (G) The average time to 10% of maximum core area for both femoral artery and cremaster muscle arteriole thrombi.

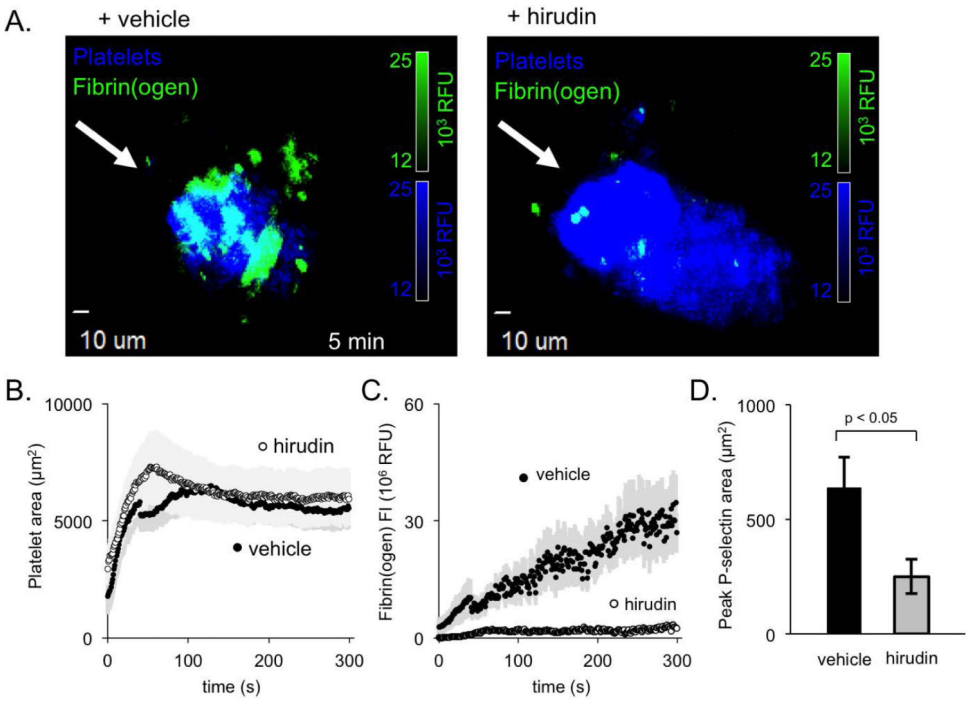

Figure 3. The role of thrombin in shaping femoral artery thrombus architecture

(A) Representative images of platelets (blue) and fibrin(ogen) (green) deposited in the presences of either vehicle (left) or hirudin (right). (B) Quantification of average platelet area and (C) fibrin(ogen) deposition for vehicle-treated (closed symbol) and hirudin-treated (open) thrombi (+/− SEM, n = 9 vehicle and 12 hirudin). (D) Average maximum P-selectin area for vehicle-treated and hirudin-treated thrombi (+/− SEM, n = 9 vehicle and 12 hirudin).

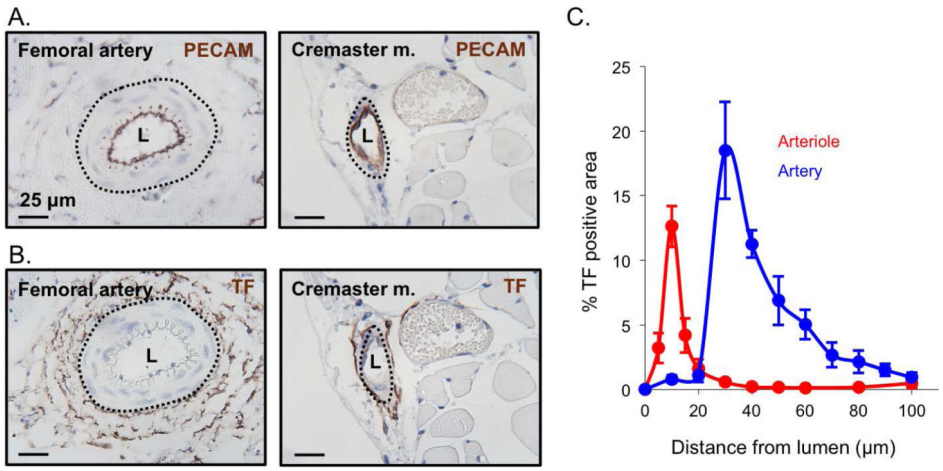

Figure 4. Tissue factor distribution in the macro- and microcirculation

Representative images of mouse femoral artery and cremaster arteriole showing (A) PECAM and (B) tissue factor staining of vessel endothelium (brown) and vessel lumen (L). (C) Quantification of the percent positive area of tissue factor radiating out from the vessel lumen center for the femoral artery (blue) and cremaster arterioles (red) (+/− SEM, n = 5 femoral and 5 cremaster).

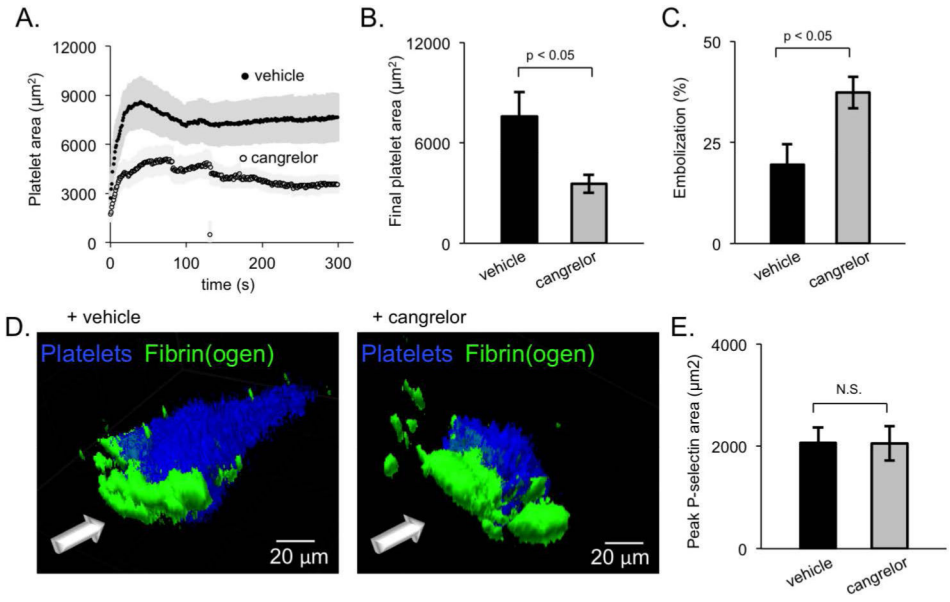

Figure 5. ADP recruits the thrombus shell during femoral artery thrombus formation

(A) Average platelet area of vehicle-treated and cangrelor-treated thrombi (+/− SEM, n = 8 vehicle and 9 cangrelor). (B) The final platelet area and (C) percent of thrombus embolization (calculated as the percent of thrombus area remaining at 300 s post-injury compared to the maximum thrombus area) for both vehicle-treated (black) and cangrelor-treated (gray) thrombi. (D) Representative 3D images of vehicle- and cangrelor-treated thrombi showing platelets (blue) and fibrin(ogen) (green). (E) The average peak P-selectin area for vehicle- and cangrelor-treated thrombi.

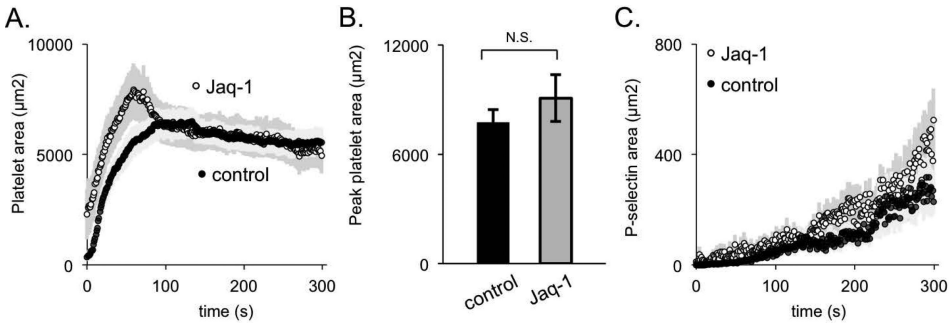

Figure 6. GPVI signaling during thrombus formation in the femoral artery

(A) Average platelet area, (B) peak platelet area, and (C) P-selectin area for control (black) and Jaq-1-treated (white or gray) thrombi (+/− SEM, n = 10 control and 12 Jaq-1 treated).

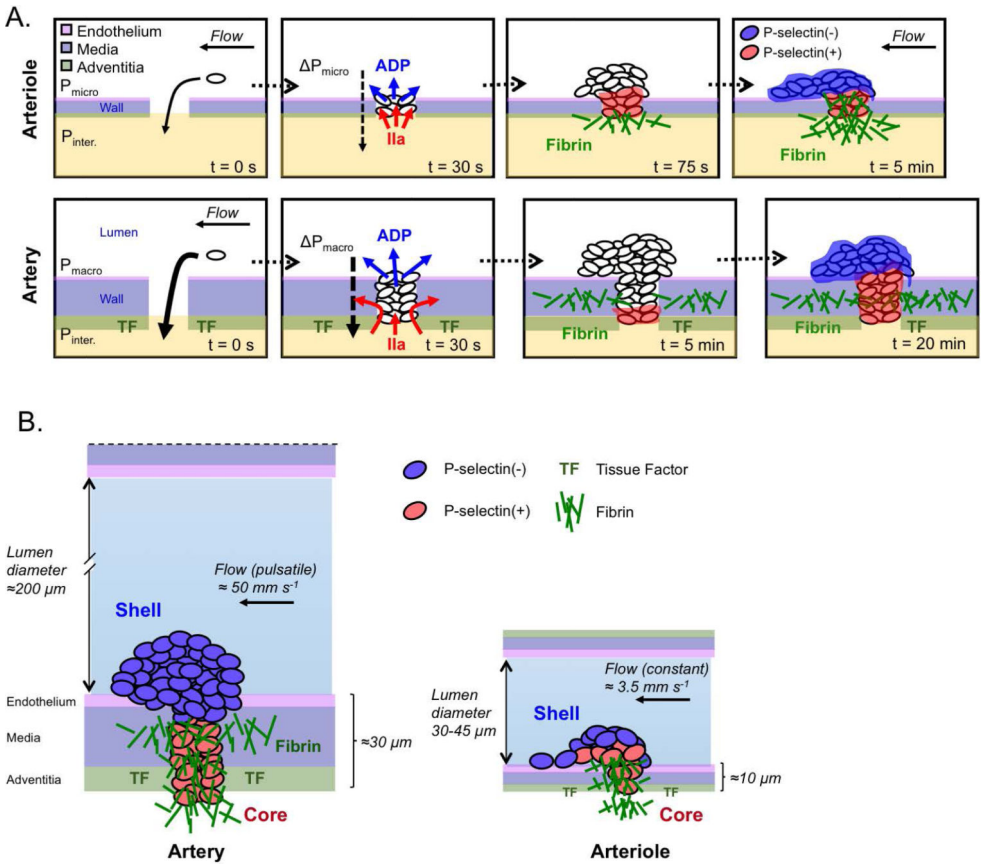

Figure 7. Model of macro- and microvasculature thrombus formation

(A) Immediately following injury blood is driven out of the vessel due to differential pressures between the macro- (P_{macro}) and microvasculature (P_{micro}) and the interstitial space ($P_{inter.}$). By 30 s after injury platelets have been recruited to the injury site, bleeding has stopped, and ADP (blue) and thrombin (IIa, red) are being produced. By ~75 s post-injury in the microvasculature thrombin has driven substantial core formation and fibrin deposition at the injury site. By 5 minutes the microvasculature thrombus has achieved its stable architecture. At 5 minutes the microvasculature thrombus has significant fibrin deposition within the vessel wall and minimal core formation, and by 20 minutes has formed a stable core/shell architecture. (B) Illustrates similarities and differences between hemostatic thrombi formed in the femoral artery (*left*) and cremaster muscle arterioles (*right*) after a penetrating injury calibrated to allow the transient escape of red cells. In both cases there was heterogeneity in the extent of platelet activation, with a shell of activated, but P-selectin(−) platelets overlying a core of P-selectin(+) platelets. In the femoral artery, the core was largely confined to the injury track within the vessel wall, extending along with fibrin into and beyond the adventitia. Thrombi formed in the femoral artery were considerably larger than those required to achieve hemostasis in the arterioles, but a smaller proportion became P-selectin(+) and the portion of the thrombus extending into the vessel lumen occupied a smaller fraction of the vessel diameter. The mean distance from the lumen

to tissue factor in the adventitia is based on the data in Figure 4. Approximate values for the flow in the arteries and arterioles are from references 22 and 9, respectively.